Invited JAST paper (Harrison and Carpick)

Atomistic Factors Governing Adhesion between Diamond, Amorphous Carbon, and Model Diamond Nanocomposite Surfaces

Pamela L. Piotrowski,[1,*] *Rachel J. Cannara,*[2,*] *Guangtu Gao,*[1] *Joseph J. Urban,*[1] *Robert W. Carpick,*[3] *and Judith A. Harrison*[1]

[1]United States Naval Academy
Chemistry Department
572 Holloway Road
Annapolis, MD 21402

[2] National Institute of Standards and Technology
Center for Nanoscale Science and Technology
100 Bureau Dr.
Gaithersburg, MD 20899

[3] Dept. of Mechanical Engineering & Applied Mechanics,
University of Pennsylvania
220 S. 33rd St.,
Philadelphia, PA, 19104-6315

*These authors contributed equally to this work.

Abstract

Complementary atomic force microscopy (AFM) and molecular dynamics (MD) simulations were conducted to determine the work of adhesion for diamond(111)(1x1) and diamond(001)(2x1) surfaces paired with other carbon-based materials. In the AFM experiments, the work of adhesion between an amorphous carbon tip and individual (001)(2x1)-H and (111)(1x1)-H crystal grains of a microcrystalline diamond sample was determined from pull-off force measurements, and by using fits to friction versus load measurements. Both methods yielded adhesion values that were larger on the (001)(2x1)-H diamond surface by 27-55%, with

the magnitude of the difference depending on the measurement method and the tip used. As well, on both surfaces, the work of adhesion for a 150 nm radius tip was found to be ~3-4 times lower than for a 45 nm radius tip. The MD simulations allowed the quantification of the influence on adhesion of variables that are not easily changed in an experiment, including hydrogen coverage, commensurability, and atomic roughness. For self-mated contacts, the average adhesion between two flat diamond(001)(2x1) surfaces calculated from the MD simulations was smaller than for self-mated diamond(111)(1x1) contacts for all hydrogen coverages examined. As well, the relative alignment of the opposing surfaces was found to significantly affect the adhesion, such that incommensurate alignment strongly reduces adhesion. Changing the counterface to an amorphous carbon surface, which more closely modeled the AFM experiment, resulted in adhesion reductions when paired with both diamond(111)(1x1) and (001)(2x1) that were of similar magnitude. Pairing model diamond nanocomposite surfaces with the diamond(111)(1x1)-H sample resulted in even larger reductions in adhesion. These results point to the importance of atomic-scale roughness in determining adhesion, a variable which is not known nor easily controlled in AFM experiments, and could be one factor contributing to the different trend in adhesion for diamond(001)(2x1) versus diamond(111)(1x1) observed in the experiments and simulations. However, the absolute values of the works of adhesion for experiment and simulation are in reasonable agreement. The calculated W values show a modest dependence on hydrogen coverage, whereby an optimal coverage is found which is intermediate to fully terminated and fully exposed. Although, fully H-terminated surfaces have a lower surface energy, removing an optimal number of H atoms reduces the work of adhesion by producing a larger mean separation between the counterface and the topmost atoms, which now include C atoms. Density functional theory calculations performed on hydrogen-terminated, single-crystal

diamond surfaces revealed small, C-H bond dipoles on both the diamond samples, with the (001)(2x1)-H surface having the larger dipole, but having a smaller dipole moment per unit area due to the lower surface density of C-H bonds. Charge separation at the surface is another possible source of the difference between the measured and calculated work of adhesion.

Keywords Adhesion, Diamond, nanocomposite diamond, amorphous carbon, diamond-like carbon, nanotribology, work of adhesion, pull-off force, atomic force microscopy, friction force microscopy, molecular dynamics, *ab initio*, density functional theory

1. Introduction

As a result of its unique electrical, mechanical, and tribological properties, diamond has been the focus of great interest both as an object of scientific study and as an ideal material for applications ranging from cutting tool coatings and waste water purifiers to chemical sensors, electronic devices, and micro- and nanoelectromechanical systems (M/NEMS). Due to its high fracture strength and chemical robustness, it can withstand exposure to harsh environments and resist mechanical wear long after most other materials fail. Thus, diamond is a potential candidate for replacing silicon for M/NEMS applications [1]. Silicon has a relatively high surface energy, is very brittle, and tends to fracture easily. The native oxide on silicon produces a hydrophilic surface that encourages water to form bridges between micro- and nanoscale objects in close proximity, often causing device failure. Hence, silicon M/NEMS surfaces typically require special coatings (*e.g.*, self-assembled monolayers) to protect these devices from the devastating effects of adhesion [2]. With these issues in mind, the adhesive properties of diamond

at the micro- and nanoscale must be investigated to determine whether diamond is superior to silicon.

The adhesive properties of any pair of materials surface can depend strongly on the atomic termination of the surfaces. *Ab initio* studies have shown that the presence of hydrogen on diamond surfaces forming an interface with a metal can reduce the work of adhesion by one order of magnitude, depending on the metal [3,4]. Density functional theory (DFT) calculations revealed that terminating the diamond or silicon surface with hydrogen produces lower surface energies than termination by oxygen or hydroxyl groups [3,5]. Moreover, in the presence of water or a mixture of water and hydrogen gases, adhesion can be reduced by causing the surfaces to be terminated with –H as opposed to terminating with –OH or =O [6]. In an atomic force microscopy (AFM) experiment, Kaibara *et al*. compared pull-off forces on H- and O-terminated patterned regions of a diamond (001) film and measured higher adhesive forces for the oxygenated region [7]. The difference was more than two-fold in air due to the higher hydrophilicity of the O-terminated regions. Indeed, the contrast decreased substantially when the sample was vacuum-annealed and then measured in an inert argon atmosphere, due to the desorption and subsequent absence of water.

Hydrogen surface termination and bulk content is also important for adhesion and tribological properties of diamond-like carbon (DLC) [8] and nanocrystalline diamond films [9,10]. Molecular dynamics (MD) simulations have shown that the removal of hydrogen atoms from self-mated diamond contacts leads to increased chemical bond formation, or adhesion [11]. In that case, covalent bonds were formed across the interface, and separation of the surfaces led to fracture. Similarly, removing the hydrogen termination from a single-crystal diamond counterface in sliding contact with DLC increased friction by increasing the formation of

chemical bonds between the counterface and the DLC [12]. More recently, the incorporation of hydrogen into DLC films was shown to reduce friction in self-mated DLC-DLC contacts [13].

By definition, the work of adhesion (W) is the energy per unit area required to separate two semi-infinite surfaces from zero separation to infinity. For two dissimilar materials, this quantity is equivalent to a sum of the surface energies, γ_1 and γ_2, of the two surfaces (because, effectively, the separation process creates the two surfaces), minus the interfacial energy, γ_{12}. Hence, $W = \gamma_1 + \gamma_2 - \gamma_{12}$, where W is also known as the Dupré energy of adhesion. To control adhesive forces between two materials, the work of adhesion can be varied by changing the surface termination. However, this assumes that the two surfaces are perfectly flat. If one or both of the surfaces is rough, then the actual area of contact will be less than the apparent contact area [14], even at the atomic scale [15-17]. Taller asperities (or protruding atoms) at the interface will prevent some of the smaller features (or other atoms) from closely approaching each other, increasing the separation between different regions of the surface and therefore reducing the energy of interaction. While the extent to which nano- or even atomic-scale roughness affects adhesion measurements is not fully understood[18], recent MD simulations indicate that the effects could be dramatic [15,16].

At present, both modeling and experiment have been used to investigate adhesion at the nanometer scale. In an AFM experiment, adhesion is measured by recording pull-off forces (L_C) between an AFM tip and a sample surface in a controlled or ambient environment. The work of adhesion is calculated from the measured pull-off force using a continuum model of contact mechanics [19]. The calculation requires assumptions or measurements made about the nature of the contact, including the range of interaction and the tip shape and size [20-22]. For linear elastic materials where the tip shape is well-described by a paraboloid, the pull-off force is directly

proportional to the product of the work of adhesion and the radius of curvature of the tip. The proportionality constant depends on the range of adhesive interactions compared with the elastic deformations caused by adhesion[21]. This in turn depends on the elastic properties of both materials. These properties may be different at a surface or for small tip shapes compared with bulk values. Moreover, small-scale roughness may go unobserved and yet completely alter the nature of the measurement. Delrio *et al.* used both experiment and numerical analysis to show that an increase in microscale surface roughness (2-10 nm) can decrease adhesive forces for nominally identical surface chemistries [23]. Luan and Robbins used MD simulations to examine the effects of tip shape and atomic-scale roughness on the work of adhesion between a tip and an atomically flat surface [16]. In that work, W decreased by a factor of 2 when the tip and surface were incommensurate and by another factor of 2 when atomic-scale roughness was introduced. Hence, surface roughness is an important parameter over a wide range of length scales, so it is important to understand its effects down to the atomic scale.

In this work, we present experimental and theoretical studies of the work of adhesion between H-terminated diamond samples of a given orientation and diamond samples paired with other carbon-based materials. For these investigations, we combined MD simulations, *ab initio* calculations, and AFM experiments. Unlike the previous *ab initio* studies that compared surface energies for H-terminated C(001)(1×1) (unreconstructed) and C(111)(1×1) [24] (in addition to those mentioned in the above discussion of surface termination), the MD simulations used here simulate the reconstructed 2×1 (001)–H surface, which is the energetically favorable structure. As well, the MD simulations account for long-range van der Waals interactions and consider the work of adhesion, not just surface energy. *Ab initio* calculations were also used to determine the presence of bond dipoles of single-crystal diamond surfaces. The work of adhesion values

obtained by MD were compared with AFM data recorded from force *vs*. displacement (LvZ) and friction measurements. The friction measurements provided information about the contact mechanics of the interface, namely, the load-dependence of the contact area. Works of adhesion could then be derived from the pull-off forces measured from both the sliding experiments and the quasistatic LvZ measurements. The AFM friction measurements used to extract the adhesion and pull-off data were reported previously in a separate paper describing similar MD and AFM comparisons of orientation-dependent friction in dry nitrogen between microcrystalline diamond (MCD) surfaces and diamond (MD) and amorphous carbon (AFM) tips formed by electron beam-induced deposition (EBID) in a transmission electron microscope [25]. Here, we glean further information from those AFM experiments for comparison with new MD simulations of adhesion and DFT calculations of surface dipoles. One result reported in the work by Gao *et al*. showed that both L_C and the sliding work of adhesion (W_{FL}) were always higher on the (001) surface than the (111) surface for both of the tips used in the AFM experiments. Because L_C and W_{FL} were both larger for the smaller tip (of radius 45 nm), with the smaller tip exhibiting roughly twice the adhesion of the larger (150 nm) tip, it was speculated that the tips had chemical differences, while any roughness differences were not considered.

Since then, Brukman *et al*. performed temperature-dependent studies in ultra-high vacuum of the friction on diamond (001) and (111) single-crystal surfaces between 25 K and 225 K using two different polycrystalline diamond (PCD) tips of radii 30 nm (Tip 1) and 60 nm (Tip 2) [26]. Sliding was along the $[11\bar{2}]$ direction on the (111) and the $[010]$ on the (001) crystal, and sample surfaces were not deliberately H-terminated. In those studies, the measured W_{FL} was lower on the (001) surface for Tip 2 for all temperatures and for Tip 1 between 90 K and 180 K. Adhesion values were very close for Tip 1 at other temperatures, and the difference in adhesion

between (111) and (001) increased for Tip 2 at temperatures below 135 K. Similar to Gao *et al.*, substantially different behavior was observed for the two tips used by Brukman *et al*. However, for both tips a similar trend and ratio of L_C values for (001) and (111) samples was observed compared with corresponding W_{FL}, indicating that the contact mechanics behavior, which relates W to L_C, was similar for the two surfaces, independent of tip shape and chemistry. Auger electron spectroscopy showed that the (001) sample surface had slightly greater oxygen coverage than (111) (0.21 *vs*. 0.16 monolayers, respectively). It is possible that the additional O- (in place of H-)termination gives rise to the difference in W_{FL} for (001) *vs*. (111), but that interpretation opposes the result of Kaibara *et al*. [7].

These previous measurements and those of Ref. [25] confirm that the nature of the tip has a strong effect not only on the magnitude of adhesion but also on the manner in which adhesion depends on the surface orientation and temperature. In addition, there is some indication that the work of adhesion (W_{LZ}) obtained from LvZ pull-off measurements differs significantly from the dynamic sliding case. In this work, previous results will be reviewed and compared with additional W_{LZ} data recorded during the experiments reported in Ref. [25]. MD simulations will also be employed to isolate the potential mechanisms responsible for these experimental observations. MD was used in Refs. [26] and [25] to study temperature-dependent friction on (001) and (111) surfaces, but adhesive forces were neglected based on the assumption that they would add a simple offset to the friction versus load data. Moreover, the goal was to deduce whether there are intrinsic differences in the shear properties of the two surfaces in the absence of chemical differences. Here, the study of the diamond samples is extended by focusing on adhesion. By combining MD simulations and *ab initio* DFT calculations with AFM experiments,

we aim to build a more complete picture of the physics and mechanics at interfaces with diamond samples.

2. MD Simulation Methods

In the MD simulations, *W* is calculated by bringing two surfaces into perpendicular contact and generating an LvZ curve. The energy of this interaction is obtained by using trapezoidal rule to numerically integrate the area enclosed by the attractive portion of the force curve. The work of adhesion is obtained by dividing the energy of interaction by the area of the computational cell (Table I). Self-mated C(111)(1×1) and C(001)(2×1) contacts were examined. The interactions of both diamond crystals with H-terminated, model diamond nanocomposite (MDN) surfaces and several amorphous carbon surfaces were also examined. A complete set of the counterface-sample pairs examined with MD is given in Table I. The nature of MD simulations also allowed for an examination of the influence of variables, which are not easily changed in an AFM experiment, including H-termination, temperature and counterface-surface alignment on *W*.

A sample MD simulation system composed of two, infinitely flat C(111)(1×1)-H surfaces is shown in Fig. 1. In this system, the counterface (upper surface) was placed approximately 10 Å away from the lower surface. Both diamond surfaces were composed of seven layers of carbon atoms and one layer of hydrogen atoms, and each surface contained 144 atoms. The dimensions of the computational cell were 30.2 Å by 26.1 Å, which corresponds to twelve diamond unit cells repeated along the $[\bar{1}10]$ lattice direction and six unit cells repeated along the $[\bar{1}\bar{1}2]$ lattice direction, respectively. Each surface was divided into one rigid and one thermostatted region. The counterface was moved toward the surface by giving the rigid atoms a constant velocity of 1 Å/ps. The rigid atoms in the lower surface were held fixed. Unless otherwise indicated, the

remaining atoms were maintained at a temperature of 300 K using the Langevin thermostat [27]. Newton's equations of motion were then integrated using a time step of 0.25 fs. Nearly identical results can be achieved when obtaining the LvZ curve, either by applying the thermostat to the gray atoms in Fig. 1 or by equilibrating the system to 300 K and then integrating the gray atoms without constraints while obtaining the LvZ curve.

As listed in Table I, seven systems were studied by MD: (i) self-mated C(111)(1×1)-H; (ii) self-mated C(001)(2×1)-H; (iii)-(iv) C(111)(1×1)-H against two different amorphous carbon counterfaces; (v) C(001)(2×1)-H against an amorphous carbon counterface; and (vi)-(vii) C(111)(1×1)-H against two different MDNs (MDN1 and MDN2). When paired with a C(111) counterface, the amorphous carbon samples were attached to diamond (111) substrates so that the periodic boundary conditions of the counterface-sample pair would be equal. One amorphous carbon counterface is composed of 94.4% sp^3-hybridized carbon, and the interface region is passivated with hydrogen [28]. The second surface is hydrogen-free and is mostly (85.3%) sp^2-hybridized carbon [13]. Both of these amorphous carbon samples have been used in our previous MD simulations of friction. The amorphous carbon sample attached to C(001) is hydrogen-free and contains 80.6% sp^2-hybridized carbon (Table I). The MDN surfaces were generated by inserting 16 H-terminated diamond (111) and (110) grains into an amorphous carbon matrix. [29] Although the identity and number of each type of grain embedded in the matrix were the same, the location and tilt varied so that films of different roughness were created. The average root-mean-square (RMS) roughness on MDN2 and MDN1 are given in Table I.[29] Snapshots of the samples are shown in Fig. 2, and the total number of atoms and dimensions of each counterface-surface pair are summarized in Table I.

The term counterface refers to the upper sample, which was always fully H-terminated, while varying degrees of hydrogen coverage on the lower samples were examined. Periodic boundary conditions were applied to the *x*- and *y*-directions (the contacting plane) for all simulations. The adaptive intermolecular reactive empirical bond-order potential (AIREBO) [30] was used to calculate the forces within the MD simulations. The AIREBO potential contains torsional terms, intermolecular terms (van der Waals' interactions), and terms for modeling covalent bonding based on the second-generation REBO potential.[31] The terms in addition to the REBO potential increase the computational time significantly. With this in mind, the simulation systems are typically designed to minimize the number of atoms used, while not adversely influencing the simulation results. Because the AIREBO potential is based on the REBO potential, it is one of a few empirical potentials with long-range forces that can model chemical reactions. Nonetheless, it should be noted that, because carbon and hydrogen have similar electronegativities, partial charges were not included in the REBO or the AIREBO potentials. Both the REBO and the AIREBO potentials have been used successfully to model mechanical properties of filled [32] and unfilled [33] nanotubes, properties of clusters [34], indentation and contact [11,17,29,35], the tribology of diamond [17,25,36] and DLC [12,13,37], stress at grain boundaries[38], and friction and polymerization of model self-assembled monolayers.[39,40]

Average *W* values for the self-mated diamond contacts were calculated by averaging data from contact simulations with independent starting configurations obtained by shifting the counterface in the contacting plane. Due to the periodicity of each system, the counterface was shifted incrementally a fraction of the lattice constant in the x and y directions. A total of 5 and 7 independent starting configurations that span the surface unit cells were examined for the C(111)(1x1) and the C(001)(2x1) samples, respectively. Both the LvZ data and *W* values were

obtained from each of these independent starting configurations. The average *W* corresponds to the average of all of the starting configurations for a given counterface-sample pair. In an AFM friction versus load (FvL) experiment, the tip is rastered over the sample (*i.e.*, each scan line is obtained by incrementing the displacement perpendicular to the sliding direction). Thus, measurements are obtained over a two-dimensional range of relative positions between the tip and sample atoms. Averaging over different starting configurations approximates the line-averaged response from an AFM experiment in sliding contact.

3. MD Results

To calculate *W*, load versus separation (LvZ) force curves were generated for each counterface-sample pair used in the MD simulation (Fig. 3). As the counterface moved toward the sample, the force on each atom within the lower sample was calculated and summed to give a total load at each timestep. The separation is the difference in the average z positions of atoms on the sample and those on the counterface closest to the interface. For the diamond samples, the average z position of the atoms closest to the interface is the average position of the terminal hydrogen atoms (or carbon atoms if the hydrogen is completely removed). The roughness of the amorphous carbon and MDN samples makes defining the surface separation more challenging. For the amorphous carbon and the MDN samples, the atom closest to the opposing sample is found. The vertical position of all atoms belonging to this sample that are within a vertical distance of this atom that is two times the roughness (Table I) are then averaged to find the average z position of the surface atoms.

Examination of the LvZ curves in Fig. 3 reveals that, when the counterface-sample pair is commensurate, the alignment (or relative position) of the two surfaces dramatically influences

the force curve. For example, when the contacting pairs are both C(111)(1x1)-H, the samples are prevented from reaching small separations when the hydrogen atoms on opposing samples are directly above and below one another. This is referred to as the "aligned" configuration. Shifting the counterface slightly so that the hydrogen-atoms are not directly above and below one another allows the counterface and the sample to get closer together, shifting the repulsive portion of the force curve to smaller separations and enlarging the attractive region of the LvZ curve, both of which ultimately impact *W*. The "shifted" configuration that ultimately leads to the lowest *W* corresponds to the one where H atoms on opposing samples are equidistant from each other in the *x*-*y* plane. This is the "shifted" LvZ curve in Figure 3. This phenomenon is also apparent in the force curves for two opposing C(001)(2x1)-H surfaces (Fig. 3). Due to the larger lattice constants on the (001)(2x1) surface, the repulsive portion of the force curve for the "shifted" configuration that leads to the lowest *W* is at a smaller separation than it is for the self-mated C(111)(1x1)-H contacts. Because *W* depends on surface alignment, force curves were generated for several different initial configurations for both the self-mated (111)(1x1) and (001)(2x1) self-mated contacts.

Substituting an amorphous carbon sample (DLC) for one of the diamond samples makes the contacting pair incommensurate. In addition, it makes the contacting interface more analogous to the AFM tip-diamond surface contact. Using MDN surfaces also makes the interface incommensurate and adds an additional component of roughness. The force curves for the interaction of two amorphous carbon counterfaces and two MDNs with C(111)(1x1)-H are also shown in Fig. 3. Comparison of data from the systems containing the two amorphous carbon samples reveals that the mostly sp^3-hybridized surface comes into closer proximity with the C(111) sample surface than the mostly sp^2-hybridized surface . That is, the repulsive portion of

the force curve is shifted to smaller separations. This is largely due to the fact that the mostly sp^3-hybridized film is hydrogen terminated, so hydrogen-hydrogen non-bonded interactions dominate, while the mostly sp^2-hybridized film is hydrogen-free so carbon-hydrogen nonbonded interactions dominate.

The two MDN samples were constructed to have different roughnesses, with MDN1 being smoother than MDN2 (Table I). Because the MDN1 surface is smoother, the repulsive wall of the potential is shifted to smaller separations and a larger number of surface atoms interact with the diamond counterface at a given separation. Thus, the attractive portion of the force curve for the MDN1 surface is significantly deeper than it is for MDN2 surface. Care must be taken when attempting a direct comparison of the force curves of systems containing the MDN samples and those containing the amorphous samples, because the simulation size (contact area) differs in these systems.

The W is calculated by numerical integration of the area enclosed in the attractive portion of the force-separation curves (Fig. 3) and then dividing by the area of the computational cell in the contacting plane (x-y plane, Table I). The work of adhesion values for the "aligned" and one of the shifted configurations of both self-mated diamond systems as a function of H-termination are shown in Fig. 4. For each of these samples, the differences in the force curves (Fig. 3) brought about by the relative positioning of the hydrogen atoms on the opposing diamond samples is reflected in the values of W shown in Fig. 4. Shifting the counterface so that its hydrogen atoms were laterally equidistant to the hydrogen atoms on the opposing surface produced the largest values of W. In this configuration, referred to as the "shifted" configuration (Fig. 4), the hydrogen atoms on opposing samples can draw nearer causing changes in the LvZ curves (Fig. 3). The average W was calculated from the W obtained from each of the independent starting

configurations. For all hydrogen coverages, the average *W* for C(111)(1×1) was larger than for C(111)(2×1). The fact that C(111)(1x1)-H has a larger calculated average *W* than C(001)(2x1)-H is because there is a higher density of atoms on the (111) surface (0.181 atoms/Å^2) than on the (001) surface (0.157 atoms/Å^2). Thus, there are more interactions contributing to the depth of the attractive portion of the force curve. If the maximum and minimum values of *W* obtained from independent starting configurations are used to construct error bars, the MD simulations reveal no statistically significant difference in the adhesion of self-mated C(111)(1×1) contacts compared to self-mated C(111)(001)(2x1) (Fig. 5).

The values of *W* for all the counterface-sample pairs examined by MD are shown in Fig. 5 as a function of surface hydrogen coverage. All all hydrogen coverages, the MDN surfaces exhibit lower values of *W* than the average values of *W* and are outside the error bars calculated for both self-mated C(001)(2×1) and C(111)(1×1) contacts. In addition, MDN2 has a lower *W* than MDN1 for all hydrogen coverages. The roughness of MDN2 is larger than it is for MDN1 and prevents it from coming into close proximity with the opposing diamond sample. As a result, the attractive portion of the force curve is very shallow (Fig. 3), which ultimately translates into small values of *W* compared to the MDN1 surface. In fact, roughness seems to be the dominate influence on *W* for both MDN samples and removing the H-termination from the MDN samples has little impact on the calculated values of *W*.

To examine adhesion between an incommensurate counterface-sample pair, amorphous carbon counterfaces were brought into contact with both C(111)(1×1) and C(001)(2×1) samples. Two different amorphous carbon (DLC) samples with different sp^2-to-sp^3 ratios were paired with C(111)(1×1) and one amorphous sample was paired with C(001)(2×1). The values of *W* as a function of hydrogen coverage of the diamond-sample surface are shown in Fig. 5. For all

hydrogen coverages and all amorphous samples examined, the values of *W* were smaller than *W* for self-mated diamond contacts.

The values of *W* for the self-mated diamond contacts exhibit small minima at hydrogen coverages around 30 to 40%. The origin of this minimum can be understood by considering the interaction between two C(111)(1×1) samples. When the surfaces are both fully H-terminated, hydrogen-hydrogen non-bonded interactions dominate. As hydrogen atoms are removed from the lower surface, there are fewer hydrogen-hydrogen non-bonded interactions for a given distance. Carbon-hydrogen non-bonded interactions replace hydrogen-hydrogen interactions as hydrogen is removed; however, the carbon atoms are farther from the hydrogen atoms on the opposing sample surface. Thus, the attractive region of the force curve decreases slightly (Fig. 6). When all of the hydrogen atoms have been removed from surface of one sample, carbon-hydrogen non-bonded interactions dominate. This causes the well depth of the force curve to increase and shift to larger separations (Fig. 6). Because the well depth has increased, the value of *W* increases.

While variable-temperature measurements are difficult to achieve experimentally, the temperature can be changed easily in MD simulations. The work of adhesion for the aligned configuration of fully-terminated, self-mated C(001)(2×1)-H and C(111)(1×1)-H contacts as a function of temperature is shown in Fig. 7. The data in Fig. 7 reveal that increasing the temperature from 100 to 700 K monotonically decreases the value of *W* by a small amount. The decrease is likely due to the effect of thermal expansion, leading to slightly larger bond separations. Brukman *et al.* [26] observed experimentally in variable temperature UHV AFM studies that on both (001) and (111) single crystals for both tips used, the work of adhesion decreased by 23 – 44% when increasing the temperature from 135 to 220 K, whereas contrasting trends with temperature were seen in the experiment for different tips in the range of 50 to 135

K.. In the MD simulations, the extrapolated change from 135 – 220 K is 155.3 – 154.5 and 200.8 – 200.1 mJ/m^2 for the C(001)(2×1)-H and C(111)(1×1)-H self-mated contacts, respectively, which is far smaller than the AFM results.

5. DFT Methods and Results

Because electrostatics are not included in the MD simulations, DFT was used to examine the partial atomic charges at the C(111)(1×1)-H and C(001)(2×1)-H surfaces to determine if differences exist in electrostatics could be a contributing factor to the differences in adhesion that are observed in AFM experiments. DFT calculations were carried out with the Gaussian03 suite of programs [41] using periodic boundary conditions. These calculations require only the coordinates for the contents of a single unit cell and the cell's dimensions. The unit cells were hydrogen-terminated on the upper and lower z-surfaces. The PBEPBE functional was employed with the 6-31G(d) basis set.

Two charge derivation schemes were used (as implemented in Gaussian03): the Mulliken population analysis,[42] and fits to molecular electrostatic potential using the CHELPG[43] method. The Mulliken method was used and found to be more reliable; thus, those results are reported herein.

Consistency was checked with a sub-set of the simulation results by comparing with the B3LYP functional (for the 100 surface), and by using explicit atom approach, where DFT calculations were performed on diamond segments (for the 111 surface). In the latter case, two system sizes, 102 and 182 atoms initially, were considered. The explicit atom calculations were single point energy calculations at the B3LYP/6-31G(d) level of theory. Overall, the results were consistent between methods within 5-15%.

The results are summarized in Table II. The hydrogen atom on the surface of the diamond sample is slightly positive for both samples, with the (100) having slightly more charge. The hydrogen-bearing carbon is slightly negative for both surfaces, again with the (100) surface having slightly more charge. The quaternary carbon is nearly neutral for both samples. The difference in charge across the bond is proportional to the bond moment. For the C-H bond, the charge difference is 0.266 and 0.286 electrons for the (111) and (100) surfaces, respectively. For the C-CH bond, the charge difference is -0.214 and -0.266 for the (111) and (100) surfaces, respectively. Thus, there are charge fluctuations in the *z*-direction for the (100) surface. However, the net charge difference per unit area depends on the density of the charge-bearing sites and corresponding bonds, which is 18.16 and 15.73 C-H bonds/nm^2 for the (111) and (100) surfaces respectively. This produces a charge difference per unit area of 4.83 and 4.49 electrons/nm^2 for the (111) and (100) surfaces respectively at the very surface (*i.e.*, from the C-H bond polarization). The C-H bond length is nearly identical for both surfaces; therefore, the electrostatic dipole per unit area produced by the C^--H^+ bonds are stronger for the (111) surface than the (100) surface. The C-C bonds in the layer below also produce a charge difference, but of opposite sign. Although this dipole reduces the effect of the C-H bond dipole, the C-C bonds are further from the interface. Therefore, the DFT calculations predict a slightly stronger electrostatic field at the (111) surface compared to (100), which would increase adhesion with neutral but polarizable groups on the counterface. It would also increase (decrease) adhesion with dipoles whose direction vector has a component parallel (anti-parallel) to the C-H bonds, essentially due to the local interaction between the charges of the outermost atoms. The AIREBO potential,[30] by virtue of its being fit to experimental data for hydrocarbon systems, captures the effect of the C-H dipole to some extent although without further investigation it is not clear how

much discrepancy there is between the AIREBO potential and the DFT calculation for diamond surfaces. Furthermore, the charge just due to the outermost H atoms is 1.93 and 1.78 electrons/nm^2 for the (111) and (100) surfaces respectively. These charges will exert a local electrostatic repulsion on positively charged H atoms on the counterface. This effect is not captured by the AIREBO potential and would tend to make surfaces with protruding H atoms repel one another more strongly than MD simulations predict, thus reducing the work of adhesion. The DFT calculation predicts the effect is slightly larger for the (111) surface compared to the (100) surface.

5. AFM Methods and Results

Achieving precise lateral alignment of tip atoms with respect to the surface periodicity for adhesion or friction measurements is extremely challenging in an AFM. Doing so requires accurate control over the tip structure and knowledge of the local surface topology. This has been achieved only in exceptional cases, such as rotational alignment of a flake of graphite attached to an AFM tip, where the sample could then be rotated.[44] This is particularly challenging on diamond surfaces. From separate measurements on single-crystal diamond, lateral stick-slip has been observed and the orientation of C(001)(2×1)-H dimer domains can change on the scale of a few to tens of nanometers (Fig. 8), consistent with previous scanning tunneling microscopy measurements.[45] Aligning tip and surface atoms laterally within an individual domain requires higher precision and stability than is typically available in an AFM, as well as knowledge of the atomic structure of the tip, itself, which is not possible in all but a few scanning probe systems. Thus, it is very difficult to determine and control local tip-sample lattice alignment in AFM LvZ

experiments, and we rely on the MD simulations for information about any dependence of adhesion on lateral tip-sample alignment.

As mentioned above, the AFM experiments included two separate measurements of adhesive (pull-off) forces, L_C. In the previous study [25], L_C values recorded during FvL measurements on individual MCD (001) and (111) crystallites, which were grown by hot filament chemical vapor deposition, were reported. These crystallites were characterized by Raman spectroscopy, X-ray photoemission spectroscopy (XPS), elastic recoil detection analysis (ERDA), and X-ray near-edge spectroscopy (XANES). The Raman spectrum showed a single sharp sp^3 peak at 1332 cm^{-1} and the absence of an sp^2 peak near 1580 cm^{-1} indicative of diamond character; the XPS exhibited a strong reduction in the oxygen signal post H-termination; ERD analysis showed the reduction of water adsorbed on the surface post termination (and air exposure); finally, the XANES spectra demonstrated diamond character and H-termination via a combination of a strong exciton and second bandgap at 289.15 eV and ~302 eV, respectively, a small amount of π-bonding indicative of graphitic bonds at grain boundaries, and the presence of a C-H shoulder near 287 eV. For all variable-load experiments, the lateral displacement of the tip along the surface that occurs in response to an applied load was compensated with piezo motion to keep the tip above the same location on the surface [46]. This tilt-compensation scheme was necessary because, while the RMS roughesses of the surfaces was 1-3 nm over a 500×500 nm^2 x-y range, the surfaces consisted of 10-50 nm islands of ~3 Å RMS roughness. Thus, it was important to confine the tip to individual islands during each measurement. Using the convenient "COS" approximation for fitting FvL data with the Maugis-Dugdale transition model,[20,21] the sliding work of adhesion was calculated, referred to as W_{FL} here. The fitting procedure for the transition model determines the behavior of a parabola-on-flat interface along a spectrum that spans the

Derjaguin-Mueller-Toporov [47] (DMT) and Johnson-Kendall-Roberts [48] (JKR) contact mechanical regimes described in Ref. [21]. By fitting the FvL data using this procedure, the way in which the contact area varies with load was determined and, thus, a value for the contact area, A_C, at the pull-off point during the experiment was obtained. Consequently, the work of adhesion is given by the equation $W = L_C/A_C$, which assumes that sliding did not induce early pull-off.

In addition to the FvL measurements that yielded W_{FL}, LvZ measurements were performed both before and after individual sets of FvL measurements on the same locations as the friction measurements. From the LvZ curves, L_C values were obtained for comparison with those obtained from the FvL experiments. Values for W_{LZ} were then calculated from these L_C values, using COS transition parameters to determine the contact area at pull-off. In the transition model, the work of adhesion is related to the pull-off force according to the equation,

$$W = \frac{-L_C}{\chi \pi R}, \tag{1}$$

where R is the tip radius, and χ is a dimensionless parameter determined from the transition model fitting procedure. Note that L_c is generally a negative quantity, but here we will treat the L_C-W relationship and discussions about L_C in terms of its magnitude, and all values of L_C reported here are positive. The values of χ range from 1.5 to 2, corresponding to the JKR to DMT regimes, respectively.

Both the W_{FL} and the W_{LZ} obtained from the two types of AFM measurements (FvL and LvZ) are reported in Table III. The experimental uncertainties in Table III correspond to the relative combined standard uncertainty of the reported value.[49] The use of continuum methods to model nanoscale contacts presents some uncertainty in the methodology,[15] and quantitative values for adhesion are important for real applications. The range of adhesion values that represent possible results from our measurements is estimated by calculating W based on two different approaches

for determining W from the measured L_C. The first approach, mentioned above, uses the COS transition parameter, χ, to identify the contact behavior with respect to the JKR-DMT spectrum. The second approach uses a physically reasonable estimate for the dimensionless Tabor parameter (μ_T), which is a measure of the ratio of the amount of deformation caused by adhesive forces relative to the counterface-surface equilibrium separation (z_0).[50] Thus, μ_T is yet another indicator of the appropriate contact mechanics regime (assuming a continuum model applies). The exact equation for Tabor's parameter is:

$$\mu_T = \left(\frac{16RW^2}{9K^2 z_0^3} \right)^{1/3}, \tag{2}$$

where $K = \frac{4}{3}\left(\frac{1-\nu_{tip}^2}{E_{tip}} + \frac{1-\nu_{surface}^2}{E_{surface}} \right)^{-1}$ is the combined elastic modulus, and ν and E are equal to Poisson's ratio and Young's modulus, respectively. Combining Eqs. (1) and (2) yields

$$\mu_T = \left(\frac{16L_C^2}{9\pi^2 RK^2 \chi^2 z_0^3} \right)^{1/3}. \tag{3}$$

Tabor's parameter ranges from 0 to 6.23, where low and high values in this range correspond to DMT and JKR contacts, respectively. Low values indicative of the DTM regime, like those observed by Brukman *et al.*, would be expected for diamond surfaces.

While it is not clear what μ_T should be for an amorphous tip on diamond, it is expected to be more JKR-like than a diamond-diamond interface because of its lower modulus and possibly

higher surface energy. With that in mind, an upper bound for μ_T for each AFM tip-sample pair was calculated by assuming JKR behavior for in Eq. (1) (*i.e.*, $\chi = 1.5$) and a relatively low value for E_{tip} of 100 GPa. Average bulk values for the elastic constants of diamond ($E_{(111)}$ = 1208 GPa, $E_{(001)}$ = 1054 GPa, $\nu_{(111)}$ = 0.047, and $\nu_{(100)}$ = 0.105) were used.[51] The z_0 were taken from the MD simulations of corresponding, self-mated diamond pairs reported here. For (001) and (111), z_0 = 1.9 Å and 1.8 Å, respectively. In comparison with the amorphous counterfaces, the diamond-diamond interfaces represented the smallest possible values of z_0 and, therefore, gave an upper bound for μ_T, which was 0.015-0.023 for C(111)(1×1)-H and 0.015-0.035 for C(001)(2×1)-H, depending on the tip. A new χ parameter was then calculated.[21] Table III displays the W_{LZ} values that were calculated using the estimated μ_T (and new χ values). In general, the work of adhesion calculated in this way represented a ~10-20% reduction in the work of adhesion compared with those calculated from the COS parameter, χ, and it moved the W_{LZ} values even further away from the corresponding W_{FL} values. The (very conservative) Tabor estimate produced more JKR-like contact behavior, but the difference was not large. Note that this result depends only slightly on E_{tip}, and inserting even the largest z_0 yields only minor changes.

5. **Discussion**

In the AFM experiments, two amorphous hydrocarbon-coated tips with different radii were used to examine the adhesion of individual diamond grains on an MCD surface in dry N_2 at room temperature. The work of adhesion was calculated from pull-off forces during force displacement curves and while performing friction *vs*. load scans. While the magnitude of W and the pull-off force depended on the measurement method, both methods yielded values of W and

pull-off force that were larger on the C(001)(2×1)-H sample than for the C(111)(1×1)-H sample. For both diamond self-mated contacts, the MD simulations produced values of W that were within the range of values measured experimentally. However, the *average* values of W calculated from the MD simulations were larger for the C(111)(1×1)-H self-mated sample. Despite the fact that simulation and experimental conditions were designed to correspond as closely as possible, the remaining differences that exist must contribute to the disagreement between AFM and MD. Possible explanations include the different contact geometry (parabola-on-flat in AFM versus two infinitely flat surfaces in MD), differences in atomic-scale roughness of the two surfaces in the experiment, electronegativity differences, and the presence of defects or impurities.

Determining the contact area from AFM data remains one of the most challenging aspects of extracting materials properties from the data for which we rely on continuum mechanics models. Recent MD simulations of Luan and Robbins have shown that continuum contact models underestimate the contact area of nanoscale single-asperity contacts, calling into question the validity of continuum models at the nanoscale [15,16]. Subsequent MD simulations revealed that this same trend exists when contact between a curved diamond tip and single-crystal diamond surfaces is simulated [25]. Although the results from continuum mechanics fits may be prone to quantitative error, a comparison of different surfaces using the same tip remains meaningful as long as roughness is a constant. In addition, in simulations with finite-sized tips, it is possible to use various definitions of contact [15,25,40,52]. Nonetheless, given the sensitivity of W to the contact area, infinitely flat surfaces were used in the MD simulations here.

The MD simulations showed that the relative position of the hydrogen atoms on opposing diamond samples results in a large variation in the calculated values of W. Substituting an

amorphous carbon counterface for a diamond counterface removes the complication of averaging over counterface-sample alignments and has the benefit of making the counterface more similar to the AFM tip. It should be noted, however, that the sp^2-sp^3 ratio in the EBID-produced AFM tip was not measured [25]. With that in mind, counterfaces with different sp^2-sp^3 ratios were used in the simulations. All the amorphous, incommensurate counterfaces lowered the calculated values of *W* compared to self-mated diamond contacts. In addition to being incommensurate with the diamond samples, the amorphous carbon counterfaces were not atomically flat. Indeed, the simulations showed that progressive roughening of one of the contacting bodies, *i.e.*, by progressing from C(111) to an amorphous sample and, ultimately, to an MDN sample, reduces the work of adhesion significantly.

The previous MD simulations of Luan and Robbins [16] and the simulations presented here demonstrate that roughness reduces the work of adhesion. It is possible that the larger AFM tip has a greater surface roughness than the smaller tip; in other words, the larger extent of the contact zone formed by the larger tip means that any rough features at the apex are more likely to prevent adjacent atoms from contacting the surface[53]. This effect may explain why the large AFM tip produced consistently lower values of *W* and pull-off force than the smaller AFM tip when paired with a given sample (Table III). Likewise, although the apparent, nanoscale roughness was the same when measured by the two tips, any differences in atomic-scale roughness between the C(001) and C(111) samples could lead to the different *W* values reported here. As seen in the scanning electron microsopy (SEM) image in Fig. 9, the (001) surface is known to grow via layer-by-layer growth[54] whereas the (111) surface grows via multiple nucleation processes [55]. It is not well understood exactly how this affects atomic-scale roughness, but it is possible that growth dominated by individual nucleation sites produces an atomic-scale

roughness that leads to lower adhesion for the (111) surface. On the other hand, the dimer rows on the (100) surface produce their own atomic-scale "roughness" of an ordered nature. Nonetheless, it is notable that the Tabor estimate produced a larger difference in comparison with the COS calculation for the (001) surface compared with the (111) surface. This discrepancy indicates that continuum mechanics models could be less valid for the (001) surface, even though from a growth standpoint the greater roughness of the (111) should lead to a greater deviation from the continuum model.

Care was taken to H-terminate the diamond samples used in the AFM experiments [25]. Thus, there should be no unsaturated carbon atoms on the sample. However, the concentration of dangling bonds on the tips is unknown. AFM measurements on ultrananocrystalline (UNCD) surfaces [10] and MD simulations of the contact of diamond and DLC surfaces have shown that the presence of unsaturated bonds increases adhesion [11-13]. In the simulations, this occurred via the formation of covalent bonds between the two contacting bodies. When both surfaces are fully H-terminated, the DFT calculations presented here show that positive charge exists at the surface due to the expected charge transfer from the H atom to the C atom. The calculated charge and bond moment for the C(001)(2×1)-H sample agrees with recently published DFT data [6]. As noted earlier, the AIREBO potential does not contain terms to model partial charges that arise from electronegativity differences. Thus, any changes in work of adhesion that arise from charges on both surfaces in proximity to one another is not captured in the MD simulations.

The addition of different atom types, such as oxygen, to the diamond surfaces could complicate the chemical reactivity and the charge landscape of the surfaces. Brukman *et al.* [26] used a variable-temperature, UHV AFM to measure the pull-off force and W between polycrystalline diamond tips and single-crystal C(111)(1×1) and C(001)(2×1). As mentioned

earlier, Auger analysis revealed the presence of less than a monolayer of oxygen on the (111) and the (001) surfaces. While the way the oxygen is bound has not been resolved, recent DFT calculations reveal that added oxygen to the C(001)(2×1) sample increases the magnitude of the bond moments at the surface. When the diamond is –OH and =O terminated, the oxygen is negative and the bond moments are 0.99e and 0.5e, respectively [6]. The existence of these partial charges is likely to influence the work of adhesion measured by Brukman *et al*. In that case, the work of adhesion measured for both C(111)(1×1) and C(001)(2×1) with the smaller PCD tip were indistinguishable near room temperature (225 K). In contrast to the trends reported here, when a larger PCD tip was used, the C(111)(1×1) surface exhibited higher adhesion. In an effort to isolate the effect of partial charges on the adhesion of H-terminated diamond, MD simulations that utilize a potential energy function with Columbic interactions are currently underway.

The MD simulations predict a slight temperature dependence of the work of adhesion such that it decreases as the temperature increases. Clear differences exist between previous variable-temperature AFM experiments [26] and the present simulations, and therefore it is not possible to conclude that the trends in the experimental and calculated work of adhesion with temperature are governed by the same phenomena.

6. Conclusion:

The origins of adhesion forces and the work of adhesion were studied by complementary atomic force microscopy (AFM) and molecular dynamics (MD) simulations. AFM measurements, using amorphous hydrocarbon tips, found that the work of adhesion was larger on the (001)(2x1)-H diamond surface by 27-55% compared to the (111)(1x1)-H surface. Although the absolute values of the works of adhesion for experiment and simulation are in reasonable

agreement, the simulations found that the average work of adhesion between two flat diamond(001)(2x1) surfaces was smaller than for self-mated diamond(111)(1x1) contacts for all hydrogen coverages examined, in contradiction to the AFM results. However, the relative alignment of the opposing surfaces was found to significantly affect the adhesion, such that incommensurate alignment of atoms strongly reduces adhesion. As this factor is not known or easily controlled in the AFM experiments, it could contribute to the different trend in adhesion for diamond(001)(2x1) *vs.* diamond(111)(1x1) observed by the experiments and simulations. Indeed, the dependence of the work of adhesion on tip size is consistent with this idea: lower work of adhesion was observed with the larger tip, and could be due to the fact that the larger tip samples more roughenss, increasing the mean separation between the surfaces at equilibrium and correspondingly decreasing the work of adhesion.

The calculated W values show a modest dependence on hydrogen coverage, whereby an optimal coverage is found which is intermediate to fully terminated and fully exposed. Although fully H-terminated surfaces have a lower surface energy, removing an optimal number of H atoms reduces the work of adhesion by producing a larger mean separation between the counterface and the topmost atoms, which now include C atoms.

DFT calculations performed on hydrogen-terminated, single-crystal diamond quantified the small positive charges at the very surface due to H atoms, with the (111)(1x1)-H surface having slightly more charge per unit area. This could act to repel a countersurface with protruding H atoms. This is another possible source of the difference between the experiment and MD simulations for the work of adhesion.

The MD simulations predict a small dependence of work of adhesion on temperature. Previous AFM measurements see the same trend over a limited temperature range but the magnitude of the effect is larger in the experiments.

While further work is needed to resolve the sources of discrepancy between AFM and MD measurements, it is clear that atomic roughness and the corresponding mean separation of the surfaces at equilibrium is a critical factor influencing adhesion at the nanometer scale, which presents both a challenge and an opportunity for understanding and controlling adhesion at small scales.

ACKNOWLEDGMENT: PLP, GAO, & JAH acknowledge support from AFOSR grant numbers F1ATA-09-086G002 and F1ATA-09-086G003 (and as part of the Extreme Friction MURI). JAH also acknowledges support from the ONR grant # N00014-09-WR20155. PLP & JAH acknowledge support from NSF grant number CMMI-0825981. RWC acknowledges support from AFOSR grant # FA9550-08-1-0024 and NSF grant number CMMI-0826076. JAH and PLP gratefully acknowledge J. D. Schall for helpful discussions. RJC and RWC gratefully acknowledge A.V. Sumant for helpful discussions and invaluable technical expertise. We also thank G. D. Wright and D. Whyte for the elastic recoil experiments, as well as D. S. Grierson and A. R. Konicek for the X-ray absorption spectroscopy measurements.

Table I. MD System Details

Counterface + Sample Pair	**Counterface Atoms C:H**	**Surface Atoms C:H**	***sp^3:sp^2:sp (%) (amorphous systems)***	***X* (Å) (unit cells)**	***Y* (Å) (unit cells)**	***Z* (Å)**	***RMS (Å)***	***Density* (g/cm^3)**
C(111)(1×1)-H + C (111)(1×1)-H	1008:C 144:H	1008:C 144:H		30.256 (12)	26.2025 (6)	14.75		
C(001)(2×1)-H + C (001)(2×1)-H	1296:C 144:H	1296:C 144:H		30.256 (12)	30.256 (12)	16.5		
sp^2-Amorphous + C(111)(1×1)-H	4008:C 0:H	1008:C 144:H	12.5 : 85.3 : 2.2	30.1777 (12)	26.135 (6)	41.5	0.57	2.75
sp^3-Amorphous + C (111)(1×1)-H	2123:C 118:H	1008:C 144:H	94.4 : 5.6 : 0	30.1777 (12)	26.135 (6)	23.8	0.48	2.86
sp^2-Amorphous + C(001)(2×1)-H	4608:C 0:H	1152:C 144:H	13.3 : 80.6 : 6.0	30.256 (12)	30.256 (12)	45	0.68	2.66
C (111)(1×1)-H + MDN1	5460:C 780:H	13179:C 461:H		65.555 (26)	65.506 (15)	27.85	1.18	
C (111)(1×1)-H+ MDN2 on C(111)	5460:C 780:H	12887:C 461:H		65.555 (26)	65.506 (15)	29.4	1.47	

Table II: Mulliken Charges on Diamond Surface Atoms (in electron units)

Atom[a]	Charge[b] (electrons)	Charge/area for the topmost H atom (electrons/nm^2)	Charge difference/area for topmost layer (eV/nm^2)
Diamond (111)			
H	0.106	1.93	4.83
C (H)	−0.160		
C	0.055		
Diamond (100)			
H	0.113	1.78	4.49
C (H)	−0.173		
C	0.093		

[a]Atoms at the surface of diamond. C (H) refers to the hydrogen-bearing carbon. C refers to the quaternary carbon beneath the hydrogen-bearing carbon.

[b]Periodic Boundary Condition Density Functional Theory (PBEPBE/6-31G(d)/auto) on unit cell.

Table III. AFM Data

Surface	Sliding direction	Tip radius (nm)	L_C from FvL (nN)	W_{FL} from COS (J/m^2)	L_C from LvZ (nN)	W_{LZ} from COS (J/m^2)	W_{LZ} from est. μ_T (J/m^2)
(111)(1×1)-H	[11-2]	45	29.7 ± 3.3	0.131 ± 0.018	23.9 ± 1.1	0.101 ± 0.008	0.093 ± 0.008
	[1-10]		25.3 ± 1.5	0.103 ± 0.009			
		150	27.6 ± 1.7	0.036 ± 0.003	23.1 ± 1.2	0.030 ± .003	0.026 ± 0.002
(001)(2×1)-H	[-110] or [110]	45	53.6 ± 2.4	0.258 ± 0.022	32.6 ± 1.3	0.157 ± 0.012	0.129 ± 0.010
		150	45.0 ± 1.7	0.064 ± 0.005	29.0 ± 1.0	0.041 ± 0.003	0.033 ±0.002
	[010]		48.1 ± 1.6	0.066 ± 0.005			

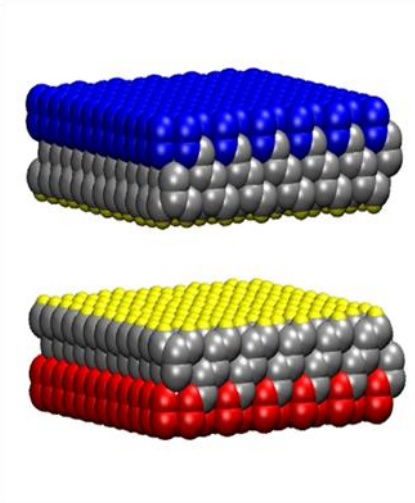

Figure **1.** Two, hydrogen-terminated C(111)(1×1)-H surfaces. Large and small (yellow) spheres represent carbon and hydrogen atoms, respectively. The red, gray, and blue spheres atoms which are fixed, thermostatted, and have a constant velocity applied to them, respectively.

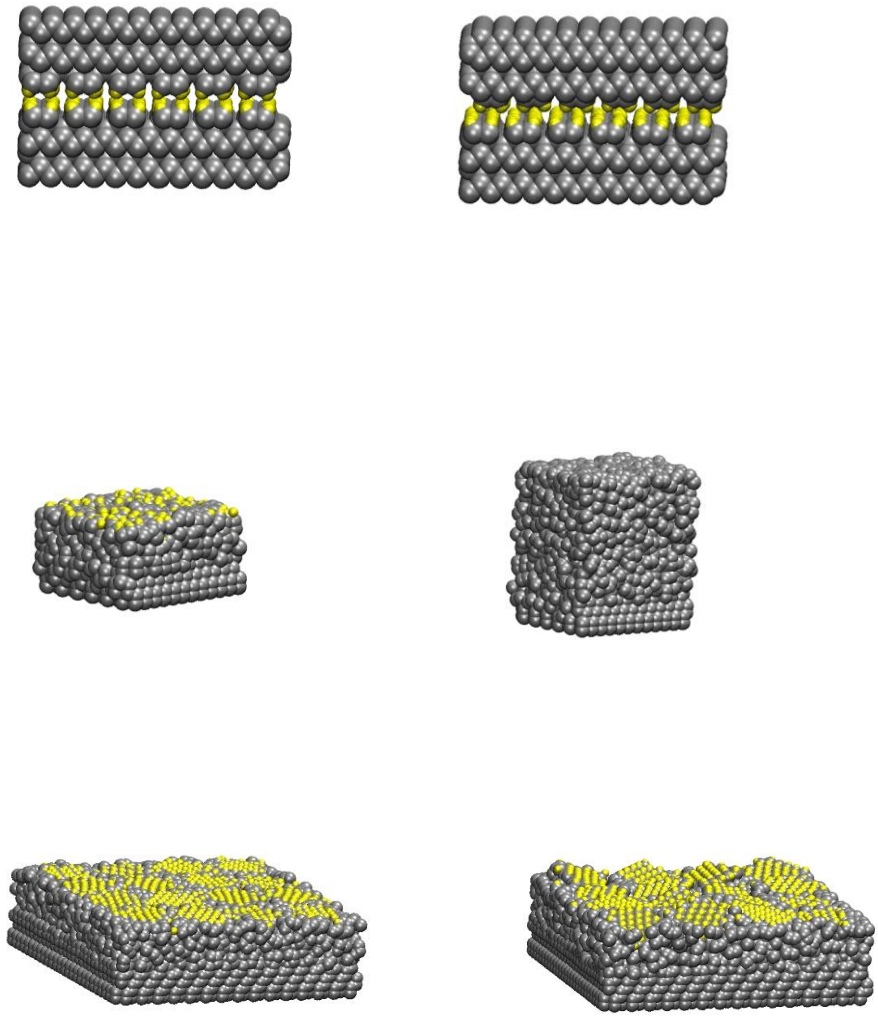

Figure 2. Sample configurations of the MD systems examined here. Gray and yellow spheres represent carbon and hydrogen atoms, respectively. In the top left and right panels, are two diamond(001)(2×1)-H surfaces in the aligned and shifted configurations, respectively. In the middle left and right panels are the sp^3-hybridized and sp^2-hybridized amorphous carbon surfaces, respectively. In the bottom left and right are the model diamond nanocomposite surfaces, MDN1 and MDN2, respectively. The numbers of atoms and dimensions for each surface are given in Table I.

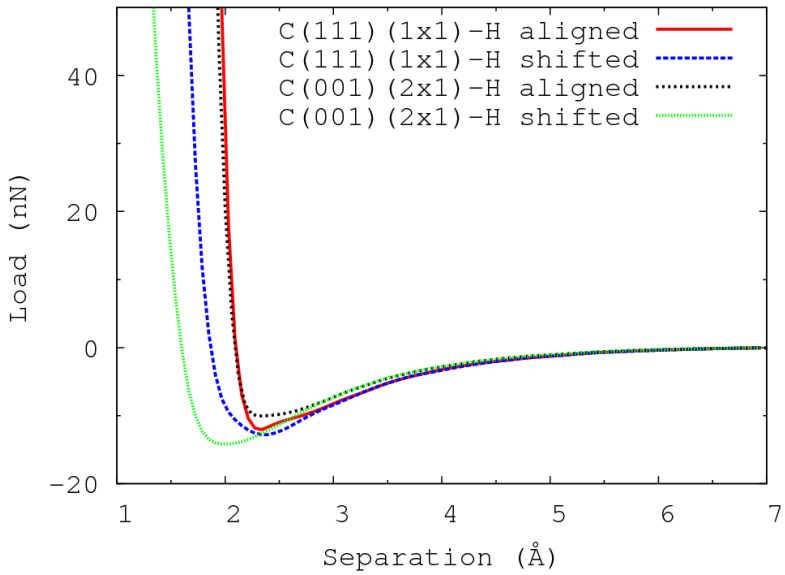
C(111)(1x1)-H aligned
C(111)(1x1)-H shifted
C(001)(2x1)-H aligned
C(001)(2x1)-H shifted
Load (nN)
40
20
0
−20
1
2
3
4
5
6
7
Separation (Å)

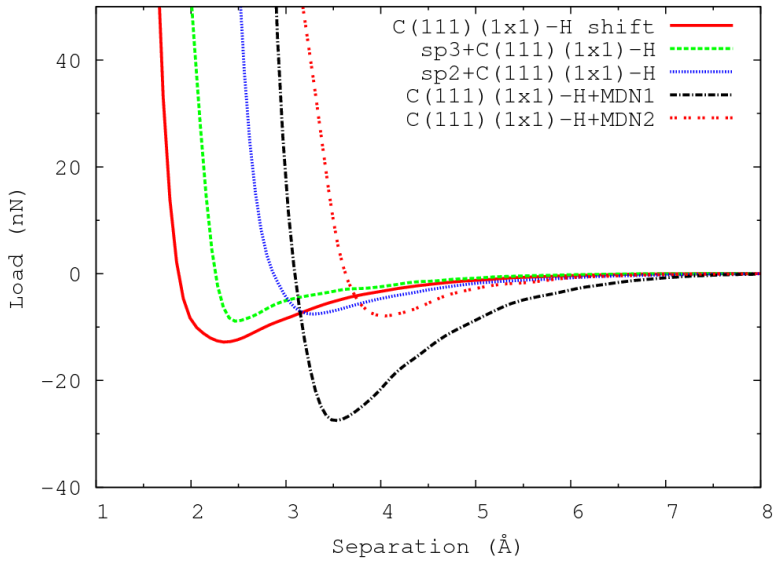

Figure 3. Load versus separation calculated from the MD simulations of the counterface-surface pair indicated in the legend. The separation is the distance between the average z position of the lowest interface atoms on the counterface and the highest interface atoms on the surface. In the upper panel, two starting configurations of self-mated diamond surfaces are shown. Both the counterface and the surface have 100% hydrogen termination. In the lower panel, the counterface-surface pair is shown in the legend.

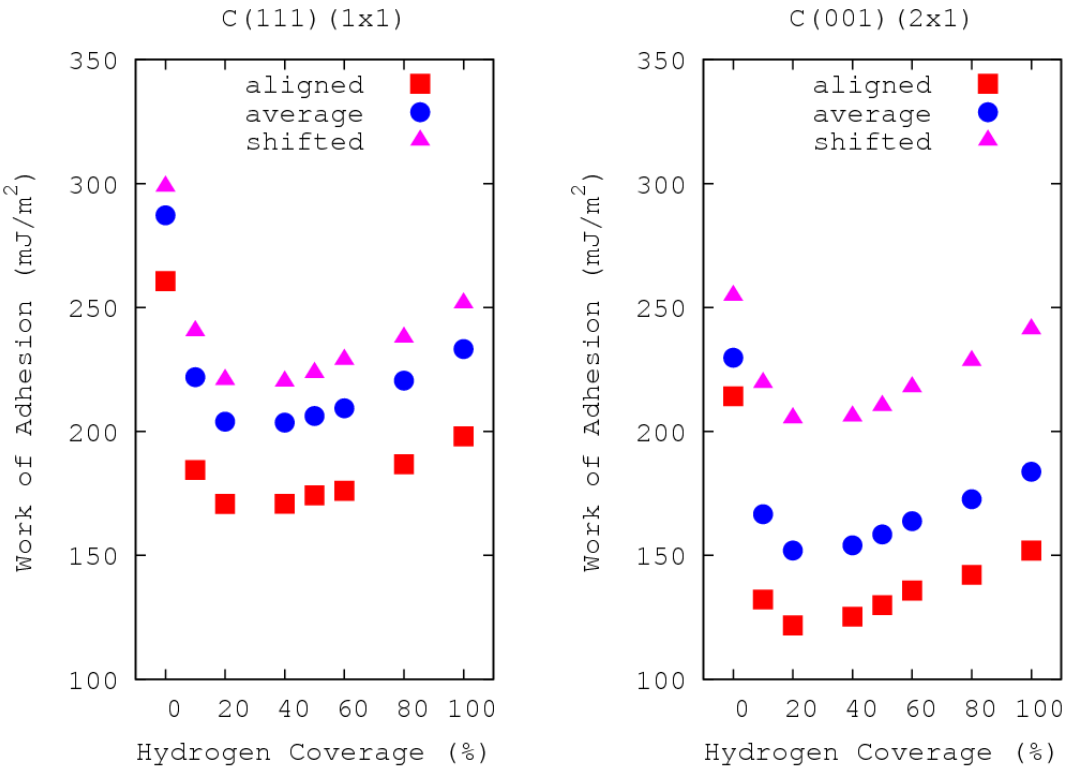

Figure 4. Work of adhesion *W* calculated from the MD simulations of self-mated C(111)(1×1) and C(001)(2×1)x1) contacts as a function of hydrogen coverage. The counterface has 100% hydrogen termination and the hydrogen-termination is varied on the lower surface. The terms "aligned" and "shifted" are defined in the text. The shifted configuration show yielded the lowest work of adhesion for that counterfacs-surface pair.

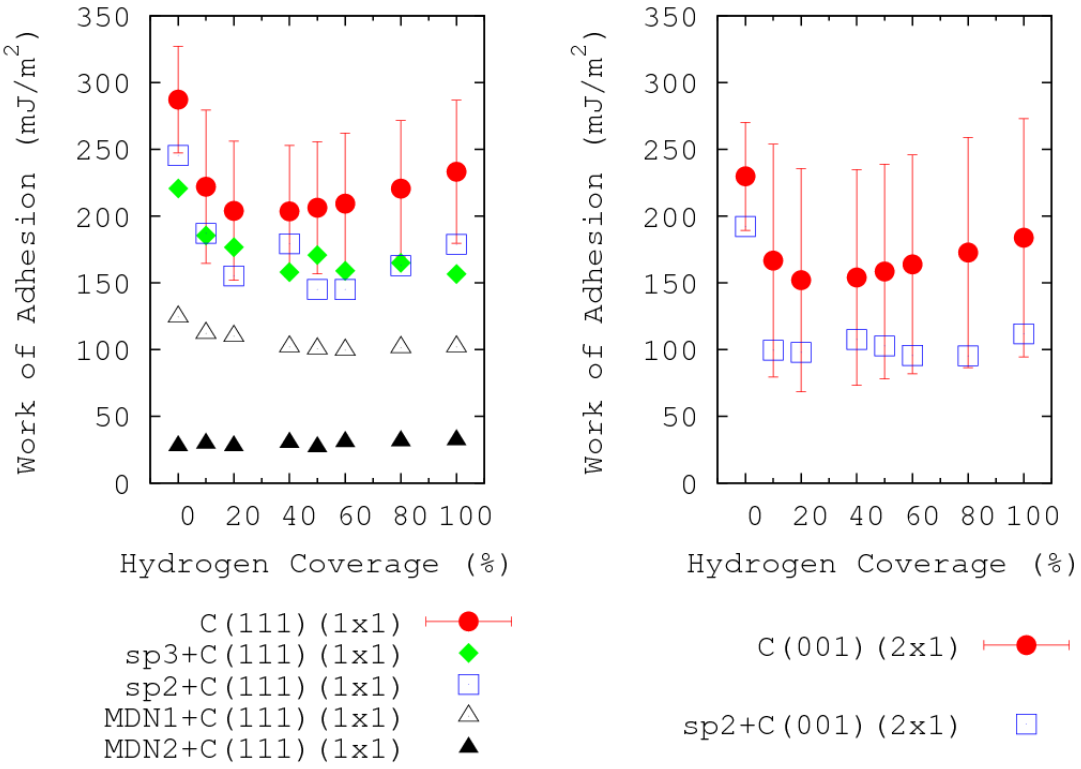

Figure 5. Work of adhesion calculated from the MD simulations for all the counterface-surface pairs examined in this work.

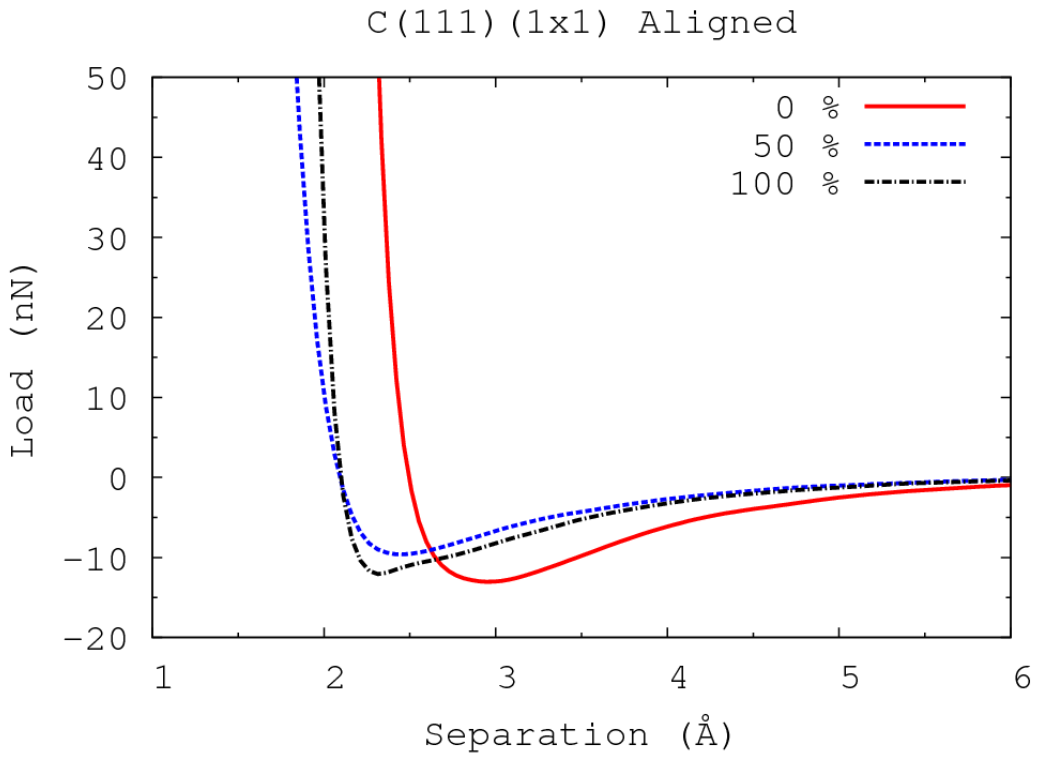

Figure 6. Load versus separation calculated from the MD simulations for the C(111)(1×1) for three different hydrogen coverages of the surface. The hydrogen atoms on opposing diamond surfaces are in the "aligned" configuration (directly above and below one another). The separation is the distance between the lowest interface atom on the counterface and the highest interface atom on the surface.

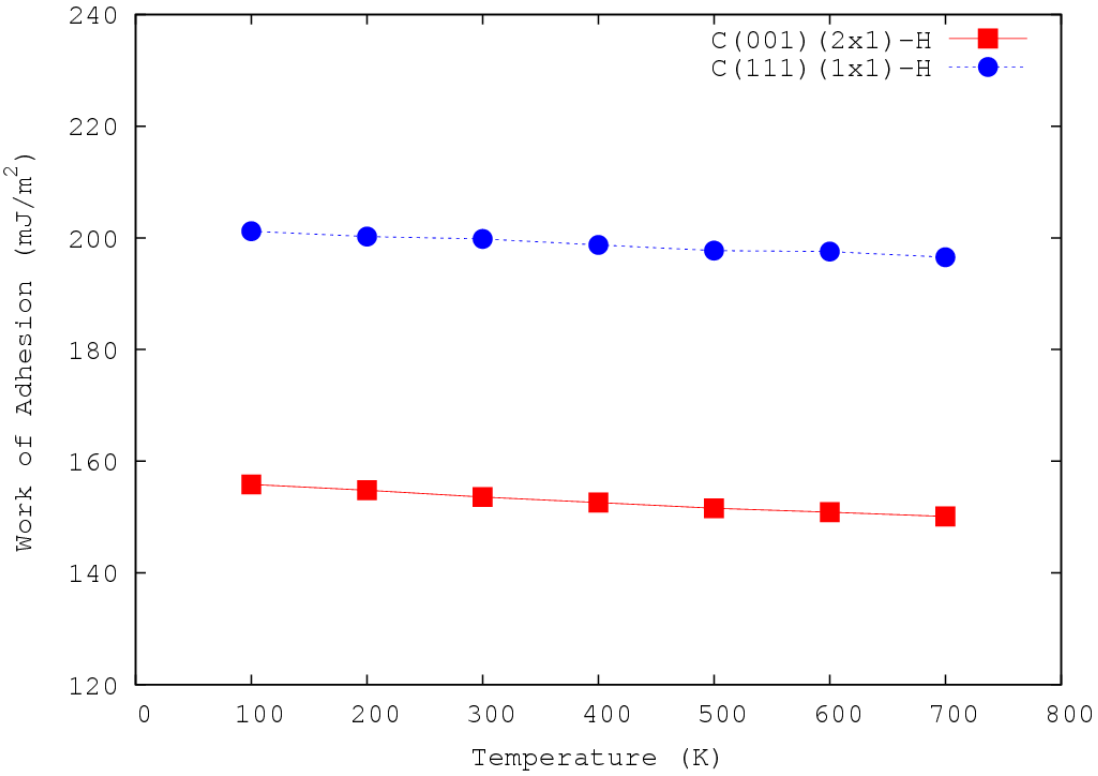

Figure 7. Work of adhesion calculated from the MD simulations for the self-mated C(111)(1x1)-H and C(001)(2x1)-H contacts as a function of temperature. The counterface and surface are in the aligned (opposing hydrogen atoms directly above and below one another) configuration and are 100% hydrogen terminated.

(a) 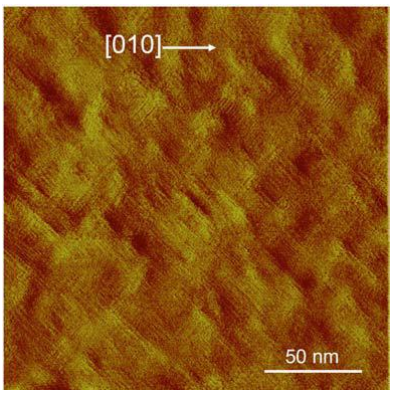

(b) 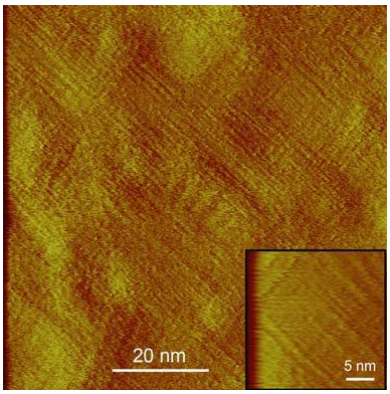

Figure 8. Lateral force images of a C(001)(2×1)-H single-crystal surface in dry nitrogen using a 45 nm EBID-coated amorphous tip. Here, the dimers are resolved, showing criss-cross patterns at 45° to the [010] sliding direction. The stick-slip periodicity is ~0.5 nm (twice the lattice constant). The image scan size in (a) is 200×200 nm^2, and the scan sizes in (b) are 80×80 nm^2 and 20×20 nm^2 (inset).

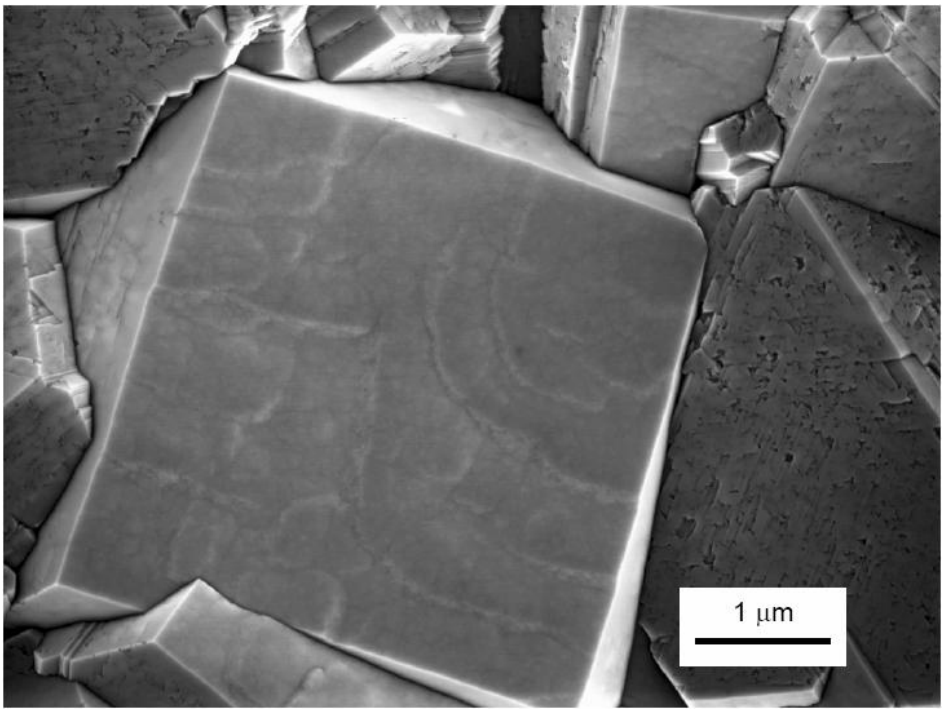

Figure 9. SEM image of the MCD surface. The terraced and triangular features are representative of the different growth mechanisms of the (001) (large central square) and (111) (triangular on right) crystallites, respectively. Possible additional figures (SEM and AFM topography)…showing adjacent (001) and (111) surfaces with their different growth mechanisms (SEM).

References:

1 O. Auciello, S. Pacheco, A. V. Sumant, C. Gudeman, S. Sampath, A. Datta, R. W. Carpick, V. P. Adiga, P. Zurcher, Z. Ma, H. C. Yuan, J. A. Carlisle, B. Kabius, J. Hiller, and S. Srinivasan, Ieee Microwave Magazine **8** (6), 61 (2007); O. Auciello, Birrell, J., Carlisle, J.A., Gerbi, J.E., Xiao, X.C., Peng, B., and Espinosa, H.D., J. Phys. C. **16**, R539 (2004); I. S. Forbes and J. I. B. Wilson, Thin Solid Films **420**, 508 (2002).

2 M. P. de Boer and T. M. Mayer, MRS Bulletin **26** (4), 302 (2001); R. Maboudian, W. R. Ashurst, and C. Carraro, 2000 (unpublished).

3 Y. Qi and L. G. Hector, Physical Review B **69** (23) (2004).

4 X. G. Wang and J. R. Smith, Physical Review Letters **87** (18) (2001).

5 G. Kern, J. Hafner, and G. Kresse, Surface Science **366** (3), 445 (1996); S. J. Sque, R. Jones, and P. R. Briddon, Physical Review B **73** (8) (2006).

6 G. Zilibotti, M. C. Righi, and M. Ferrario, Physical Review B **79** (7) (2009).

7 Y. Kaibara, K. Sugata, M. Tachiki, H. Umezawa, and H. Kawarada, Diamond & Related Materials **12**, 560 (2003).

8 A. Erdemir, Surf. Coat. & Technol. **146**, 292 (2001).

9 A. V. Sumant, D. S. Grierson, J. E. Gerbi, J. Birrell, U. D. Lanke, O. Auciello, J. A. Carlisle, and R. W. Carpick, Advanced Materials **17** (8), 1039 (2005).

10 A. V. Sumant, D. S. Grierson, J. E. Gerbi, J. A. Carlisle, O. Auciello, and R. W. Carpick, Physical Review B **76** (23) (2007).

11 J. A. Harrison, Colton, R.J., White, C.T., and Brenner, D. W., Mat. Res. Soc. Symp. Proc **239**, 573 (1992); J. A. Harrison, D. W. Brenner, C. T. White, and R. J. Colton, Thin Solid Films **206** (1-2), 213 (1991).

12 G. T. Gao, Mikulski, P. T., and Harrison, J. A., J. Am. Chem. Soc **124**, 7202 (2002).

13 J. D. Schall, G. Gao, and J. A. Harrison, J. Phys. Chem. C, submitted (2009).

14 D. L. Liu, J. Martin, and N. A. Burnham, Applied Physics Letters **91** (4), 043107 (2007).

15 B. Q. Luan and M. O. Robbins, Nature **435**, 929 (2005).

16 B. Q. Luan and M. O. Robbins, Phys. Rev. E **74**, 026111 (2006).

17 Y. F. Mo, K. T. Turner, and I. Szlufarska, Nature **457** (7233), 1116 (2009).

18 T. S. Chow, Physical Review Letters **86** (20), 4592 (2001).

19 B. Cappella and G. Dietler, Surface Science Reports **34** (1-3), 1 (1999).

20 R. W. Carpick, Ogletree, D.F., Salmeron, M., J. Colloid Interf. Sci. **211**, 395 (1999).

21 D. S. Grierson, E. E. Flater, and R. W. Carpick, J. Adhesion Sci. & Technol. **19**, 291 (2005).

22 D. Maugis, Langmuir **11** (2), 679 (1995); U. D. Schwarz, J. Colloid Interf. Sci. **261**, 99 (2003).

23 F. W. Delrio, M. P. De Boer, J. A. Knapp, E. D. Reedy, P. J. Clews, and M. L. Dunn, Nature Materials **4** (8), 629 (2005).

24 A. A. Stekolnikov, Furthmüller, J. and Bechstedt, F., Phys. Rev. B **65**, 115318 (2002).

25 G. T. Gao, R. J. Cannara, R. W. Carpick, and J. A. Harrison, Langmuir **23** (10), 5394 (2007).

26 M. J. Brukman, G. T. Gao, R. J. Nemanich, and J. A. Harrison, Journal of Physical Chemistry C **112** (25), 9358 (2008).

[27] S. A. Adelman, Adv. Chem. Phys. **44**, 143 (1980).

[28] G. T. Gao, P. T. Mikulski, G. M. Chateauneuf, and J. A. Harrison, J. Phys. Chem. B **107**, 11082 (2003).

[29] J. D. Pearson, G. Gao, M. A. Zikry, and J. A. Harrison, Computational Materials Science, in press (2009).

[30] S. J. Stuart, A. B. Tutein, and J. A. Harrison, J. Chem. Phys. **112**, 6472 (2000).

[31] D. W. Brenner, O. A. Shenderova, J. A. Harrison, S. J. Stuart, B. Ni, and S. B. Sinnott, J. Phys. C. **14**, 783 (2002).

[32] B. Ni, S. B. Sinnott, P. T. Mikulski, and J. A. Harrison, Phys. Rev. Lett. **88**, 205505 (2002); H. Trotter, R. Phillips, B. Ni, Y. H. Hu, S. B. Sinnott, P. T. Mikulski, and J. A. Harrison, Journal of Nanoscience and Nanotechnology **5** (4), 536 (2005).

[33] B. I. Yakobson, Brabec, C.J., Bernholc, J., Phys. Rev. Lett. **76**, 2511 (1996).

[34] D. W. Brenner, Dunlap, B. I., Harrison, J. A., Mintmire, J. W., Mowrey, R. C., Robertson, D. H., and White, C. T., Phys. Rev. B **44**, 3479 (1991).

[35] J. A. Harrison, S. J. Stuart, D. H. Robertson, and C. T. White, J. Phys. Chem. B **101**, 9682 (1997).

[36] J. A. Harrison, and Brenner, D. W., J. Am. Chem. Soc **116**, 10399 (1994); J. A. Harrison, G. Gao, J. D. Schall, M. T. Knippenberg, and P. T. Mikulski, Philosophical Transactions of the Royal Society a-Mathematical Physical and Engineering Sciences **366** (1869), 1469 (2008); J. A. Harrison, C. T. White, R. J. Colton, and D. W. Brenner, Phys. Rev. B **46**, 9700 (1992); M. D. Perry and J. A. Harrison, J. Phys. Chem. **99**, 9960 (1995).

[37] G.-T. Gao, Mikulski, P. T., Chateauneuf, G. M., and Harrison, J. A., J. Phys. Chem. B **107**, 11082 (2003); S. L. Zhang, G. Wagner, S. N. Medyanik, W. K. Liu, Y. H. Yu, and Y. W. Chung, Surf. Coat. & Technol. **177-178**, 818 (2004).

[38] O. A. Shenderova and D. W. Brenner, Physical Review B **60** (10), 7053 (1999).

[39] G. M. Chateauneuf, Mikulski, P. T., Gao, G. T. and Harrison, J. A., J. Phys. Chem. B **108**, 16626 (2004); P. T. Mikulski, G.-T. Gao, G. M. Chateauneuf, and J. A. Harrison, J. Chem. Phys. **122**, 024701 (2005); P. T. Mikulski and J. A. Harrison, J. Am. Chem. Soc **123**, 6873 (2001); A. B. Tutein, Stuart, S. J. and Harrison, J. A., Langmuir **16**, 291 (2000).

[40] M. T. Knippenberg, P. T. Mikulski, B. I. Dulnap, and J. A. Harrison, Phys. Rev. B **78**, 235409 (2008).

[41] M. J. Frisch and e. al., Gaussian03, Revision C.02 (Wallingford, CT, 2004).

[42] R. S. Mulliken, Journal of Chemical Physics **23**, 1833 (1955).

[43] C. M. Breneman and K. B. Wiberg, Journal of Computational Chemistry **11** (3), 361 (1990).

[44] M. Dienwiebel, G. S. Verhoeven, N. Pradeep, J. W. M. Frenken, J. A. Heimberg, and H. W. Zandbergen, Physical Review Letters **92** (12) (2004).

[45] T. Frauenheim, U. Stephan, P. Blaudeck, D. Porezag, H. G. Busmann, W. Zimmermannedling, and S. Lauer, Physical Review B **48** (24), 18189 (1993); R. E. Stallcup, Villarreal, L.M., Lim, S.C., Akwani, I., Aviles, A.F., Perez, J.M., J. Vac. Sci. Technol. B **14**, 929 (1996).

[46] R. J. Cannara, Brukman, M.J., Carpick, R.W., Rev. Sci. Instrum. **76**, 053706 (2005).

[47] B. V. Derjaguin, V. M. Muller, and Y. P. Toporov, J. Colloid Interf. Sci. **53**, 314 (1975).

[48] K. L. Johnson, K. Kendall, and A. D. Roberts, Proc. R. Soc. Lond. A **324**, 301 (1971).

[49] B. N. Taylor and C. E. Kuyatt, http://physics.nist.gov/Pubs/guidelines/TN1297/tn1297s.pdf (1994).

[50] J. A. Greenwood, Proceedings of the Royal Society of London Series a-Mathematical Physical and Engineering Sciences **453** (1961), 1277 (1997).

[51] C. A. Klein, Mat. Res. Soc. Bull **27**, 1407 (1992); J. Turley and G. Sines, J. Phys. D: Appl. Phys. **4**, 264 (1971); E. S. Zouboulis, Grimsditch, M., Ramdas, A.K., and Rodriguez, S., Phys. Rev. B **57**, 2889 (1998).

[52] M. Chandross, C. D. Lorenz, M. J. Stevens, and G. S. Grest, Langmuir **24** (4), 1240 (2008).

[53] K. S. Kim, Hurtado, J.A., FRACTURE AND STRENGTH OF SOLIDS, PTS 1 AND 2 KEY ENGINEERING MATERIALS **183-1**, 1 (2000).

[54] V. P. Godbole, A. V. Sumant, R. B. Kshirsagar, and C. V. Dharmadhikari, Applied Physics Letters **71** (18), 2626 (1997).

[55] A. V. Sumant, C. V. Dharmadhikari, and V. P. Godbole, Materials Science and Engineering B-Solid State Materials for Advanced Technology **41** (2), 267 (1996).